Reports

On the Prediction of the El Niño of 1986–1987

T. BARNETT, N. GRAHAM, M. CANE, S. ZEBIAK, S. DOLAN, J. O'BRIEN, D. LEGLER

Three different classes of numerical models successfully predicted the occurrence of the El Niño of 1986–87 at lead times of 3 to 9 months. Although the magnitude and timing of predicted ocean surface temperatures were not perfect, these results suggest that routine prediction of moderate to large El Niño events is feasible. The key to the success of the models lies in recognizing or simulating the low-frequency, large-scale changes in the tropical ocean–atmosphere system that give rise to El Niño events.

THE EXTENDED PERIODS OF UNUSUally warm sea surface temperature (SST) that occur periodically off the coast of South America are often referred to as El Niño events. We now know that these SST changes are part of far larger variations in the global climate system often referred to as El Niño–Southern Oscillation, or ENSO, events. Perhaps the largest such event in this century occurred in 1982–83, with little apparent warning but with considerable consequences for a sizable fraction of the world's population (*1*).

In the aftermath of the 1982–83 event, several scientists, using rather different techniques, showed that key features of the event could have been predicted in advance (*2–5*). In response to these scientific results, the Tropical Ocean Global Atmosphere (TOGA) program, which was designed to study the ENSO phenomenon, organized a series of experimental forecast efforts aimed at alerting the oceanographic and atmospheric communities if another event appeared likely to occur. Between late winter and spring of 1986, three different objective schemes predicted a moderate warming of the equatorial Pacific SSTs, an El Niño, to begin in late summer to early fall of 1986. Results presented below indicate these forecasts were generally successful (Figs. 1 and 2). An explanation for the success of the three rather disparate forecast procedures is also given.

The models used in the forecasts can be thought of in a hierarchical structure. The simplest conceptual physical model uses a statistical approach and invokes a balance between the zonal wind stress over the tropical Pacific and the zonal gradients in the density field of the equatorial ocean as represented by simple indices, such as regional SST or sea level. The relation between these fields is expressed in a sophisticated statistical model (denoted M1) designed to predict SST from prior variations in the tropical Pacific surface wind field, the global sea level pressure field, or both. The statistical modeling uses a substantially upgraded variation of canonical correlation analysis to find the optimal linear combination of variations in space and time in the wind or pressure field that can forecast subsequent SST change. The model is "form-free" in that the previous variations in wind and SST determine the structure of the model (*5, 6*). A variant of this approach was used by Barnett (*2*) to show that the 1982–83 event was predictable in advance of its occurrence; Graham *et al.* (*5*) extended this work, showing that skillful forecasts could be expected operationally at lead times of 1 month to greater than 1 year.

The results of two statistical models will be shown. One model (M1A) used the 6 months of wind field data prior to an initial time t_0 to forecast SST out to 6 months beyond t_0. A second model (M1B) used the prior four seasons of data on the global sea level pressure (SLP) field to forecast SST. The models had high cross-validation skills out to lead times of 5 months and four seasons, respectively, for forecasts of SST in the time frame from late summer to winter. The models generally had no appreciable skill for spring–early summer forecasts.

Increased model sophistication is introduced by expressing the ocean's response to varying wind stress in terms of the physical laws that govern that response. In this forecast scheme, denoted M2, the ocean physics are described in terms of a linear transport model on an equatorial β-plane that is wind-driven, has one layer, and incorporates reduced gravity (*7*). In such a model the tropical ocean is treated as a light (warm) dynamic upper layer that overlies a heavy (cool) lower layer that is at rest. The model's geometry extends from 18°N to 12°S and 126°E to 76°W, that is, the entire span of the tropical Pacific (Fig. 1). The meridional boundaries are taken to be solid walls, and open boundary conditions are applied at the north and south boundaries to permit free passage of coastal Kelvin and Rossby waves. Observed wind stress drives the model, and numerous results (*7, 8*) suggest that this relatively simple physical formulation, which is linear and without thermodynamics, is capable of reproducing many observed features of ENSO events.

In the forecast mode, the model is integrated up to an initial time t_0 by using observed winds. Forecasts for times beyond t_0 are made by assuming that the wind field in the future will be identical to that last given at t_0. The model is then integrated ahead for 3 months under this assumption. The model's forecast skill, like the M1 models, is highest in the last half of the calendar year.

The model does not predict SST but rather a closely related variable, the thickness of the upper layer of the ocean, denoted ULTA. The prediction of an El Niño event is based on forecast of ULTA off South America and is given in binary form, that is, an event will or will not occur with a certain probability. This decision-making process, which is derived from inspection of model performance over a prior record, was used previously by Inoue and O'Brien to demonstrate the predictability of the 1982–83 event (*3*). That same work gives the operational definition of an El Niño event used to construct the prediction rules. This prediction scheme has been used routinely since early 1985.

The third forecast scheme, denoted M3, uses a numerical model to simulate the evolution of the coupled ocean and atmosphere system in the tropical Pacific (*9*). The ocean component of M3 is similar to M2, the most important differences being the addition of an Ekman layer (to concentrate wind-driven currents near the surface) and thermodynamics (to simulate the heating of the atmosphere by the sea). The surface currents are determined by adding the Ekman velocity to the geostrophic velocity estimated by dynamics much like those in M2. Although the dynamics are linear, the SST anomaly evolution equation is fully nonlinear [that is, there are interactions between the variables governing the evolution of SST anomalies (such as vertical and horizontal ocean currents) and the SST

T. Barnett and N. Graham, Climate Research Group, Scripps Institute of Oceanography, La Jolla, CA 92093. M. Cane, S. Zebiak, S. Dolan, Lamont-Doherty Geological Observatory of Columbia University, Palisades, NY 10964.
J. O'Brien and D. Legler, Mesoscale Air-Sea Interaction Group, Florida State University, Tallahassee, FL 32306.

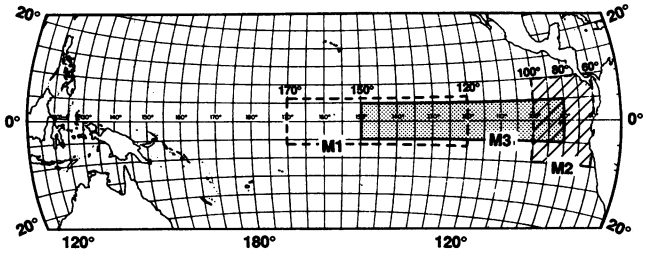

Fig. 1. Location map showing the regions for which sea surface temperature (SST) is forecast by the various models.

anomalies themselves; further, there are important interactions between the mean and anomalous components of the system]. Anomalous surface heating of the atmosphere is taken to be linearly proportional to the anomalous SST, but SST anomalies are functions only of currents and upper layer thickness. Hence all SST anomalies are dynamically forced by surface wind stress anomalies.

The atmospheric component of M3 calculates surface wind anomalies in response to SST anomalies and has steady-state dynamics and a nonlinear heating parameterization. This parameterization simulates the warming of the atmosphere by latent heating associated with precipitation and depends on both the prescribed SST and the surface wind convergence calculated within the model. The performance of the atmospheric model is described elsewhere (*10*). In the coupled mode, the atmospheric heating will depend on the model ocean SST field, which in turn is determined by winds generated by the atmospheric model.

Anomalies in tropical heat content are crucial in determining the evolution of ENSO events in M3 (*4, 9*). Fields of this variable are therefore an essential initial condition for forecasting El Niño episodes. Since the necessary information is not available from direct observations, these fields are calculated by using the model itself. To accomplish this, the model is forced by observed winds for a period of time preceding t_0, and the state resulting at t_0 is used as the initial condition for the forecast. To this point the procedure is much like M2 (*11*). However, after t_0 both the atmosphere and ocean evolve as determined by the dynamics of the coupled model, whereas M2 assumes a constant state for the surface winds and only the oceanic features evolve. In still greater contrast, M1 neither uses nor creates information between t_0 and the verification time.

In actual operation, a new M3 forecast is made every month. The results presented here and previously were obtained by a simple average of the forecasts from six consecutive months prior to t_0. Previous experimental forecasts show that the best agreement with observations is in the boreal winter, the same situation found in models M1 and M2.

Each model presents its forecast in a different format, but we have tried to express them in a way that will allow meaningful intercomparison. We present "short-range" forecasts characterized by lead times of 3 months and "long-range" forecasts at lead times of 9 months. Further, we concentrate on SST forecasts for regions of the eastern equatorial Pacific (Fig. 1). Each model predicts for a slightly different area. Past results (*5, 12*) suggest that the central area is the easiest to predict and the eastern the most difficult, but the differences are modest.

The forecasts produced by models M1 (A and B), M2, and M3 are shown in Fig. 2. Note that during some months a particular model offered no forecast (nf) due to poor expected performance at these times; the performance index depending on the statistical significance of the model.

The 3-month lead statistical model based on surface wind data (M1A, Fig. 2A) successfully captured the onset of the 1986–87 event in the Pacific, although the predicted initial peak was 1 month later than observed. The magnitude of the event in 1986, nearly 2 standard deviations, was also well forecast. The model does forecast the continuation of the event through 1987, although the warming is underestimated, particularly in the spring (a time when the model does not perform well on its training set). The secondary peak (September 1987) is forecast only moderately well, as its observed magnitude ($>2\sigma$) is substantially underestimated.

The equatorial Pacific Ocean model (M2) successfully forecast an event to occur in July 1986 from data up to the end of May 1986 (Fig. 2A). Forecasts issued prior to this time correctly indicated that no event would occur. Since a smoothing over 3 months is done to eliminate high frequencies, the discrepancy between the forecast event arrival time and the observed upswing in SST is minor, particularly given the somewhat open, poorly resolved definition of the start of an event. Continued integrations with M2 suggested that the event would die out during the spring of 1987 (it did not) and resume again in late 1987 (a successful forecast).

The coupled tropical ocean–atmosphere model (M3, Fig. 2B) appears to have simulated the onset and evolution of the event through the first half of 1986 relatively well

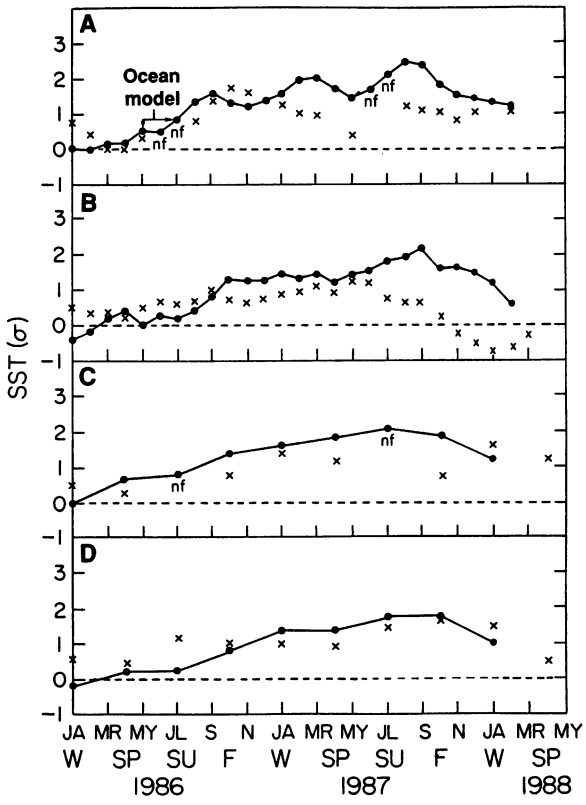

Fig. 2. (**A**) Forecasts at 3-month lead times by the model M1A versus observations. The symbol "nf" indicates no forecast and occurs when the prediction model does not show statistically significant skill. The arrow labeled "ocean model" shows the time (May) when model M2 forecasted an El Niño to occur during the next 3-month period centered on July. (**B**) Three-month lead forecasts by model M3 versus observations. (**C**) Nine-month lead forecasts by model M1B versus observations. (**D**) As in (C), but from model M3.

(*13*). After that time, the simulated and observed SST diverge as the coupled model predicts an end to the event by September 1987. In fact, equatorial SSTs returned to near normal values in the spring of 1988, about 6 months later. As with the M2 model, the wind data used to drive the model did not show the needed anomalies in the late spring and early summer. A possible early indication of problems with the forecast were the large errors in initial conditions at this time (*14*).

Mid-1987 is the least successful period for all three short-range forecast schemes. It is unusual for warm episodes to persist through the spring as in 1987. Although it is possible that the poor forecasts are caused by errors in the wind data, they may also result from omissions in the physics or statistical assumptions underlying the models.

Note that during the course of the 1986–87 event, a simple persistence forecast (that is, a forecast that calls for the current conditions to continue unchanged) would be a successful competitor with the models discussed here (of the three forecast models, only M3 makes explicit internal use of the persistence of tropical SST). However, by its nature, persistence could not have predicted the start of the event as did the models M1 through M3. Furthermore, the near constancy of the event during late 1986 and 1987 is unusual, so persistence appeared to be more effective as a forecast scheme during this event than it would during more typical events.

Models M1B and M3 produced the 9-month in-advance forecasts of the normalized seasonal SST anomalies given in Fig. 2, C and D. The model M2 has not been tested at this lead time. The statistical model forced by the global SLP field produced good results for the central Pacific SST, picking up the warming in the fall of 1986 with a forecast made at the end of February 1986 (*15*). The eventual magnitude of the event was also fairly well forecast through 1987 and early 1988, although the predicted decrease in fall was not observed, and as is typical for statistical models, there is a tendency for underestimation. As an aside, the predictions made for lead times of 6 months with this model have forecast errors that are smaller by a factor of 2 than those inferred from Fig. 2C.

The coupled model forecasts started the warming about one season too early, but from the fall of 1986 on, it performed relatively well. The model forecasts were slightly too low during much of 1987, but recovered by fall to give a clear indication of the second peak. We would judge that M3 has done better at this longer lead time than at 3 months (Fig. 2B). Over a larger set of cases (1970 to 1985) the performance of the 3-month lead is only marginally superior, being significantly better only for the early fall. The failure to improve at short lead time is an indictment of the initialization procedure; the additional information given the model is almost as likely to throw it off track for a short time as it is to help. In a particular case, perhaps including 1987, the short lead forecast may be victimized by a burst of poor data at times near t_0; the longer lead forecast has more time to recover from such problems.

All of the forecast models successfully predicted major aspects of the 1986–87 El Niño event despite the wide disparity in model type, initialization procedure, and so forth. This somewhat surprising result can be understood by realizing that ENSO is a long-period cycle: the coupled ocean-atmosphere system travels on a closed trajectory through a multidimensional phase space that is largely determined by its large-scale, low-frequency behavior. It may be buffeted about by smaller scale weather, intraseasonal tropical oscillations, and such, but beyond some point, it is so firmly locked onto the path pointing toward El Niño conditions (or toward non–El Niño conditions) that at a given time that it can no longer be deflected. All of the prediction schemes considered are able to detect such states [and in the case of M3 to simulate the system's further evolution with sufficient accuracy (*16*)].

At all times the ocean-atmosphere evolution is interactive, with low-frequency ocean and atmospheric components dominating the evolution. In principle, the ENSO signal could be detected in either medium (*17*), but the atmospheric observations are more numerous and for now the models have relied on them alone. Schemes M2 (tropical ocean model) and M3 (coupled tropical ocean–atmosphere model) convert a time series of atmospheric states into an oceanic state, whereas M1 works directly with atmospheric states. The analysis given below extracts the most important signatures of such states by performing a generalized inverse calculation with the statistical models (M1). Thus we solved for the average space-time structure of the wind-pressure fields that gave the best possible SST forecast skill (*5, 6*). We focused on forecasts for the winter season for the SLP model and November for the wind model since these were times when the models performed best. Lead times of three seasons and 4 months were selected, but the conclusion are insensitive to these choices.

Consider first short-term predictability derived from knowledge of the tropical Pacific surface wind field. The way in which the anomalous zonal wind component must evolve from February through July to give a successful forecast for SST in region M1 (Fig. 1) in November is shown in Fig. 3. Positive (westerly) anomalies are needed as early as February in the western equatorial Pacific to ensure a good forecast. This wind anomaly intensifies slowly as one approaches July, the cutoff time (t_0) for a 4-month lead forecast. The anomalous wind patch,

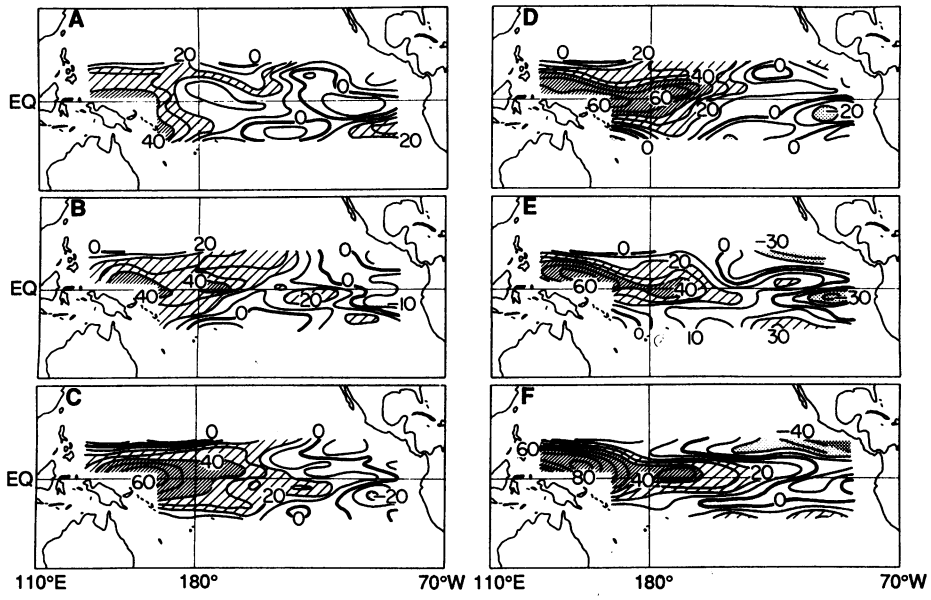

Fig. 3. Evolution of the equatorial zonal wind required for successful SST prediction. The positive values indicate eastward-directed anomalies of the zonal wind. The importance of a given month's wind information to the subsequent prediction was (**A**) February, 15%; (**B**) March, 13%; (**C**) April, 17%; (**D**) May, 19%; (**E**) June, 16%; and (**F**) July, 20%. In this case, prediction is made for November with model M1A with data ending in July (4-month lead forecast).

which initially (February) covers much of the western and central Pacific, extends eastward, particularly along the equator, as summer approaches. Yet to first order, the growth of the predictive wind anomaly is slow, and its geographic shape changes little with time. The relative importance of each month's wind data to the subsequent skill is shown numerically in the legend to Fig. 3. These numbers range from 13 to 20%, so all months are of approximately equal value to the forecast. Thus it is the large-scale, low-frequency variation in the near-equatorial wind field that gives rise to the predictive skill found in the statistical model.

The success of M2 and M3 for short-range prediction can be understood in the light of this result. Both integrate the wind information from before t_0 into the ocean state at t_0. Model M2 then assumes that the anomalous wind observed at t_0 will persist for 3 months. This is a fairly good assumption, since the predictive signal is independent of higher frequency events, for example, "west wind bursts" (Fig. 3), so that the model does well. The model M3, which evolves the wind for 3 months, has enough skill at the low frequencies and large space scales to capture the essential features of Fig. 3, that is, the near constancy of the forcing wind stress field. In addition, in both M2 and M3, remotely forced oceanic signals (such as equatorial Kelvin waves) are allowed to propagate during the 3-month forecast lead time.

The inverse calculation that uses the long-range SLP-based model (M1B) showed the manner in which the global SLP field must evolve to produce an El Niño and a successful winter SST forecast (Fig. 4). The main features of the SLP evolution are:

1) Expansion and intensification of positive SLP anomalies from Asia at t_0 minus three seasons (summer) to their almost total coverage of the Eastern Hemisphere at forecast time t_0 (spring).

2) Eastward translation of the negative SLP anomalies from the Indian Ocean into the South Pacific and their apparent unification with similarly signed Northern Hemisphere anomalies, so that by t_0 much of the Western Hemisphere is covered by below normal SLP.

3) The results discussed in the two points above, of course, represent at t_0 one phase of the Southern Oscillation. Note, however, that there is much more activity associated with the SLP field than just that of a tropical Indo-Pacific event, and that this variation is much like a global natural mode of SLP described by Barnett (*18*) and by Graham *et al.* (*5*).

4) Additional calculations have indicated that the pattern seen at t_0 (spring) grows in intensity, in place, through the summer and into the winter, and looks like the amplification of a standing wave in the atmosphere.

The above discussion and results (Fig. 4) show that the large-scale, low-frequency variations of the global SLP field are responsible for the predictive skill of model M1B. Indeed, the numerical importance of each season's information to the subsequent forecast (given as a percentage in the legend to Fig. 4) are essentially equal. Given the difference in spatial character of the SLP fields in the year preceding an ENSO event, a forecast model must capture the evolution of the anomaly field to be successful at lead times as long as 9 months.

Model M3 (coupled ocean-atmosphere) exhibits forecast skill at lead times even longer than 9 months (*4*). In the light of the discussion above, this result implies that to produce a good forecast, the coupled model must evolve its climate state along a trajectory in phase space near that of the real ocean-atmosphere system. In addition, since M3 only treats the tropical Pacific region, the interactions in this region must be sufficient to determine the system's future trajectory (*19*). This fact may seem to contradict the results shown in Fig. 4, where the relevant patterns clearly extend into other areas. Indeed, the above interpretation of Fig. 4 represents only one possible scenario. Based on M3, one could also argue that changes occurring in the Pacific, especially the western Pacific, will influence the atmosphere over the Indian Ocean and elsewhere, giving a signal there that is easier to detect in the data than the one more directly involved in the Pacific interactions. Other scenarios involving redistributions of oceanic mass within the Pacific Basin could also explain the forecast skill (*4, 9, 17, 20*). At this stage of our understanding, we cannot say which, if any, of these interpretations is correct. What we do know is that any useful long-range forecast of ENSO events must account for the evolutionary aspects of the atmosphere shown in Figs. 3 and 4.

The ability of the various models described here to produce successful forecasts of El Niños appears to be derived from the low-frequency, large-scale evolution of characteristic patterns in the atmospheric circulation. This evolution can be thought of as a signal that precedes El Niño events. The models M1 and M2 can be thought of as special types of filters designed specifically to detect this signal from given atmospheric input. The model M1 uses optimal detection filters, whereas M2 is a detection filter constrained by physical laws. The model M3 is designed to replicate the predictive signal itself and can be thought of as a type of "self-detection" filter; again, one constrained by physical laws.

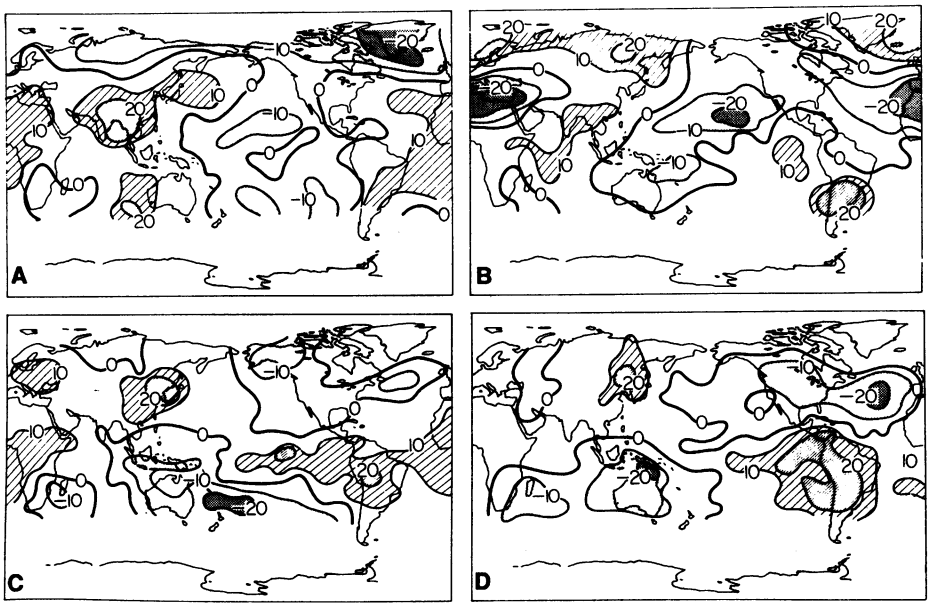

Fig. 4. Evolution of the global SLP field required for successful 9-month in-advance forecast of winter SST in region M1. The last data used in the model are from spring (t_0). The evolution of the SLP field in the year prior to t_0 is shown in the panels. Positive values indicate higher than normal SLP whereas negative values indicate lower than normal SLP. The importance of a given season's SLP information to the subsequent prediction was (**A**) spring (t_0), 26%; (**B**) winter ($t_0 - 1$), 27%; (**C**) fall ($t_0 - 2$), 22%; and (**D**) summer ($t_0 - 3$), 25%.

REFERENCES AND NOTES

1. T. Y. Canby, *Natl. Geogr.* **165**, 144 (1984); M. H. Glantz, *Oceanus* **27**, 14 (1984).
2. T. P. Barnett, *Mon. Weather Rev.* **112**, 1404 (1984).
3. M. Inoue and J. J. O'Brien, *ibid.*, p. 2326.
4. M. A. Cane *et al.*, *Nature* **321**, 827 (1986).

5. N. E. Graham *et al.*, *J. Geophys. Res.* **92**, 14251 (1987); N. E. Graham *et al.*, *ibid.*, p. 14271.
6. T. P. Barnett and R. Preisendorfer, *Mon. Weather Rev.* **115**, 1825 (1987).
7. A. J. Busalacchi and J. J. O'Brien, *J. Geophys. Res.* **86**, 10901 (1981); *J. Phys. Oceanogr.* **10**, 1929 (1980).
8. M. Inoue *et al.*, *J. Geophys. Res.* **92**, 11671 (1987); A. J. Busalacchi and M. A. Cane, *J. Phys. Oceanogr.* **15**, 213 (1985).
9. S. E. Zebiak and M. A. Cane, *Mon. Weather Rev.* **115**, 2262 (1987).
10. S. E. Zebiak, *ibid.* **114**, 1263 (1986).
11. Both M2 and M3 use the wind analyses produced at Florida State University.
12. T. P. Barnett, *J. Phys. Oceanogr.* **11**, 1043 (1981); ——— and J. Hasselmann, *Rev. Geophys. Space Phys.* **17**, 949 (1979).
13. This appears different from the forecast given in Cane *et al.* (*4*), where the magnitude exceeds the observed. The discrepancy is partly due to the difference in lead times, but is mostly attributable to the fact that the results shown here have been scaled so that the models forecast from the period from 1970–85 match the observed mean and variance.
14. The model is initialized using only wind data and so can be verified against SST observations at the time t_0.
15. Persistence forecasts of this lead time are very poor and offer no competition for M1 and M3.
16. In fact, M3 solutions will, over a matter of years, follow fairly self-similar orbits in phase space just like the actual ENSO signal.
17. W. B. White *et al.*, *J. Phys. Oceanogr.* **15**, 386 (1985); W. B. White *et al.*, *ibid.*, p. 917.
18. T. P. Barnett, *J. Atmos. Sci.* **42**, 478 (1985).
19. Models M1A and M2 also rely only on changes in the tropical Pacific for their predictive skill.
20. P. S. Schopf and M. J. Suarez, *J. Atmos. Sci.* **45**, 549 (1988); N. E. Graham and W. B. White, *Science* **240**, 1293 (1988).
21. The authors are grateful to two anonymous reviewers whose comments were helpful in improving the original draft of this paper. This work was supported by NSF grant ATM85-13713, NOAA (TOGA) grant NA85AA-D-AC132, and the NOAA Experimental Climate Forecast Center grant NA86-AA-D-CP104 to the Scripps Institution of Oceanography; by NOAA (TOGA) grant NA87-AA-D-AC081 to Lamont-Doherty Geological Observatory; and by NSF grant OCE84-15986 to Florida State University. The support of the U.S. TOGA Project Office and the Experiment Climate Prediction Program were essential to the cooperative nature of this work.

1 February 1988; accepted 18 May 1988

Irregular Recurrence of Large Earthquakes Along the San Andreas Fault: Evidence from Trees

GORDON C. JACOBY, JR., PAUL R. SHEPPARD, KERRY E. SIEH

Old trees growing along the San Andreas fault near Wrightwood, California, record in their annual ring-width patterns the effects of a major earthquake in the fall or winter of 1812 to 1813. Paleoseismic data and historical information indicate that this event was the "San Juan Capistrano" earthquake of 8 December 1812, with a magnitude of 7.5. The discovery that at least 12 kilometers of the Mojave segment of the San Andreas fault ruptured in 1812, only 44 years before the great January 1857 rupture, demonstrates that intervals between large earthquakes on this part of the fault are highly variable. This variability increases the uncertainty of forecasting destructive earthquakes on the basis of past behavior and accentuates the need for a more fundamental knowledge of San Andreas fault dynamics.

LARGE EARTHQUAKES OCCUR ALONG the San Andreas fault northeast of Los Angeles about every 131 years (*1–4*). Unfortunately, error inherent in standard radiocarbon measurements limits resolution of individual intervals between earthquakes to about ±100% of the average interval. This imprecision hampers assessment of the annual probability of a large earthquake on the San Andreas fault in southern California. If, for example, intervals vary from the mean by no more than 10%, then the chance of such an event within the next 30 years—131 to 161 years since the great 1857 earthquake—is almost 100%. If, on the other hand, intervals vary from 50 to 300 years (*2*), then forecasting major earthquakes on the basis of average intervals is less reliable. Such variability would also nurture doubts about hypotheses of uniform fault strain accumulation and relief.

On the basis of historical information and new, high-precision radiocarbon measurements, the latest three large earthquakes on the San Andreas fault near Los Angeles occurred in A.D. 1857, 1785 ± 32, and 1480 ± 15 (*4*). The two most recent events occurred during the lifetime of many trees growing along the fault. We examined growth rings of these trees to date precisely the second most recent event and to estimate its fault rupture length.

That trees are affected by large earthquakes is well known (*5*). Tree damage is even a criterion for assigning shaking intensities of VIII and above on the modified Mercalli intensity scale (MMI) (*6*). Such high intensities are typically limited to within a few kilometers of the seismic source, that is, the earthquake fault. Earlier investigators have successfully used trees to study earthquakes (*7, 8*), and a detailed review of dendroseismologic studies is in Sheppard and Jacoby (*9*).

The 1857 San Andreas rupture segment traverses three forested areas (Fig. 1); we reconnoitered each for old trees. The southernmost area, in and northwest of Wrightwood, contained the most promising trees. Sixty-five old Jeffrey pines (*Pinus jeffreyi* Grev. and Balf.), two white firs [*Abies concolor* (Gord. and Glend.) Lindl. ex Hildebt.], and three incense-cedars [*Libocedrus decurrens* (Torr.) Florin.] growing either in or around the fault zone were cored at breast-height with 5-mm-diameter corers. Cross sections were also collected from several stumps.

Using standard dendrochronological techniques (*10*), we cross-dated all cores and sections both within and between trees and with the Mill Creek Summit chronology (*11*), a tree-ring index series developed from nearby big-cone Douglas-fir [*Pseudotsuga macrocarpa* (Vassey) Mayr] (Fig. 1). We cross-dated each core by locating particularly narrow rings produced during droughts in 1782, 1795, 1809, 1813, 1823, 1841, 1843, 1845, 1857, and 1864. We then measured all ring widths to the nearest 0.01 mm with a computerized dendrometer (*12*). Missing rings were evident in some cores and were assigned widths of zero following dendrochronological procedures (*10*). Consecutive missing rings were evident in two trees that lost most of their crowns at some point in time. The most probable time for trees to cease radial growth is just after severe trauma, such as major crown loss (*13*). Hence, zeros were assigned for those missing rings immediately following the onset of trauma.

We combined measured ring-width series from trees growing away from the fault zone in a single control chronology for the period A.D. 1600 to 1900 by the use of autoregressive standardization (*14*) (Fig. 2, uppermost plot). This chronology corresponds well with other tree-ring chronologies from throughout southern California (*11*); only regional phenomena (typically climatic fluctuation) produce variations in control chronologies.

Nine conifers sampled in the Wrightwood area suffered unusual trauma, as indicated by suppressed ring growth, beginning in 1813 (Fig. 2). In all but one of these trees, this suppression was the greatest growth anomaly during their life-spans (*15*). Four trees (Pool Tree, Lone Pine Canyon, Wrightwood 3-1, and Wrightwood 3-2)

G. C. Jacoby, Jr., and P. R. Sheppard, Tree-Ring Laboratory, Lamont-Doherty Geological Observatory, Palisades, NY 10964.
K. E. Sieh, Division of Geological and Planetary Sciences, California Institute of Technology, Pasadena, CA 91125.